11

Innovative Membrane Deformable Mirrors

S. Bonora[1], U. Bortolozzo[2], G. Naletto[1,3] and S.Residori[2]
[1]*CNR-IFN, Laboratory for UV and X-Ray and Optical Research, Padova,*
[2]*INLN, Université de Nice-Sophia Antipolis, CNRS, Valbonne,*
[3]*Department of Information Engineering, University of Padova, Padova,*
[1,3]*Italy*
[2]*France*

1. Introduction

Nowadays adaptive optics (AO) is a very powerful technique for several scientific and technological applications, and with important economical perspectives. In the last decade, AO technology has fostered new solutions to improve adaptive components performance. While the scientific line has grown up quickly, AO has not experienced yet a wide spread commercial diffusion because a reasonable trade-off between performance and costs of adaptive components has not been found yet. This aspect makes AO a technology very attractive but still under development. In fact, many different AO technologies have been studied in the last years, as for example electrostatic membranes, electromagnetic fields, piezoelectricity, electro-striction, liquid crystals, MEMS etc. All these new technologies have peculiar properties which make them very useful and interesting for specific applications; however, the "universal" component, the one which could simultaneously satisfy all the requirements, has not been found yet.

To demonstrate its large and still undiscovered potentialities, we can remember that AO is presently a source of a wealth of experimental activities in scientific applications, as witnessed by the recent rich literature. In some cases AO is a totally new experimental tool which brings unexpected results; in others, its addition to experimental setup is the key for increasing the system performance. The main limitation of AO in many research activities is that AO systems still often require specialized operators, space for allocating devices and dedicated control PC/drivers.

In the last decade the benefit of AO in scientific experiments has been largely demonstrated. The main topics which have received a strong impulse from the introduction of deformable mirrors (DM's) are astronomy (Hardy, 1998), optical communications (Tyson, 1999), microscopy (Rueckel et al., 2006), quantum engineering (Bonato et al, 2008), coherent control (Bartels et al., 2000, Bonora et al., 2010), and femtosecond lasers for pulse compression (Brida et al., 2010) and focalisation (Villoresi et al., 2004). However, the use of DM's in these experiments differs case by case: in fact, each experiment has its own specific requirements depending on correction speed, system stability, amount and resolution of the correction and beam size. For this, recent researches report on the realization of many different DM

technologies (Dalimier & Dainty, 2005) in order to address either higher stroke (Bonora & Poletto, 2006), or higher resolution (Bifano, 2011; Bortolozzo et al., 2010), or different shapes.

Among the several AO recent technological developments, we can highlight the capability of deforming a correction mirror in a suitable way, but without having the information about the actual necessary deformation to optimally correct the wavefront. On this respect, let us remind as an example that the most classical AO scientific application, that is astronomy, uses DM's to reduce the impact of atmospheric turbulence on image quality; since this is a rapidly variable and a-priori unknown phenomenon with frequencies up to a few kHz, usually the DM deformation is commanded by means of the information provided by a fast wavefront sensor (WS) which monitors in real time the difference between the actual and the ideal wavefront. Such AO systems need the real-time knowledge of the deformation to be induced to the DM, and could not work without a WS. On the other hand, there are many other AO applications where the necessary mirror deformations are nearly static, and for which the use of WS can just be an additional experimental complexity (Rueckel et al., 2006). In these cases, it can be more convenient to monitor just an experimental parameter, and to optimize a suitable merit function depending on it. For this and other reasons, sensorless AO techniques (that is AO setups which do not use a WS) have been developed, obtaining extremely good results, usually at the expenses of only a reduced correction speed. Among the others, the sensorless AO techniques which makes use of optimization algorithms have been very successful: for example, since their first use (Judson & Rabitz 1992) random search algorithms (genetic, simplex or simulated annealing algorithms) demonstrated to be very effective in femtosecond lasers for both parametric amplifiers pulse compression (Bartels et al., 2000), focalization (Villoresi et al., 2004), and microscopy (Wright et al., 2007). Also the capability of realizing a fast analysis of a reference point image has been successfully used in some applications (Naletto et al., 2007; Grisan et al., 2007).

Among the various techniques developed during the last years to realize deformable optics, membrane DM's is probably becoming the most popular one, because of its extremely valuable performance and potentialities, its relative easiness of use, its handiness, and its low price. Presently, membrane DM's have been successfully used in many scientific applications, such as visual optics and laser focalisation or femtosecond laser compression experiments, and can now be found either in round or rectangular shape (see Fig. 1). Thanks to the rapid increase of fields of applications, and to the continuous technological development, it is reasonable to expect a rapid expansion of their use also in more diffused and commercial applications.

The technology of electrostatic membrane DM's consists in realizing a thin metal (silver, gold or aluminum) coating over a nitrocellulose, polyamide or silicon membrane. The membrane is then usually pre-tensioned and glued over a metallic frame (Bonora et al., 2006), and the frame is finally faced to the electrode pads by means of calibrated spacers to maintain the nominal distance between membrane and electrodes. The number of electrodes usually ranges between 19 and 64, to form a round or rectangular footprint as illustrated in Fig. 1. The electrodes are connected to a voltage amplifier which generates independent voltage signals between 0 V and 300 V. The membrane DM controller has to independently manage variable voltages for all the electrodes, on the basis of the information provided either by a suitable WS or by the adopted sensorless technique.

1.1 Applications of deformable membrane mirrors

Many are the scientific applications in which membrane DM's are presently successfully used. As an example, (Villoresi et al., 2004, Bonora et al., 2011b) reports on the optimization of laser high order harmonics generation (HHG) by the interaction of a femtosecond laser beam and a gas jet. In these experiments, the HHG signal is generated by the multi-photon ionization of gas atoms driven by the strong electric field of the laser. This extreme non-linear effect is very sensitive to laser intensity, and both WS and sensorless AO techniques have been used to improve laser focalisation. Fig. 2 shows the differences between the two experimental setups used for the optimization of the laser focusing, with and without WS. These experiments demonstrated that the sensorless technique can be very performing, even if the convergence of the algorithm requires a very high signal stability and a high laser repetition rate. To be effective in this kind of setup, fast DM systems based on embedded electronics architecture have been developed (Bonora et al., 2006a).

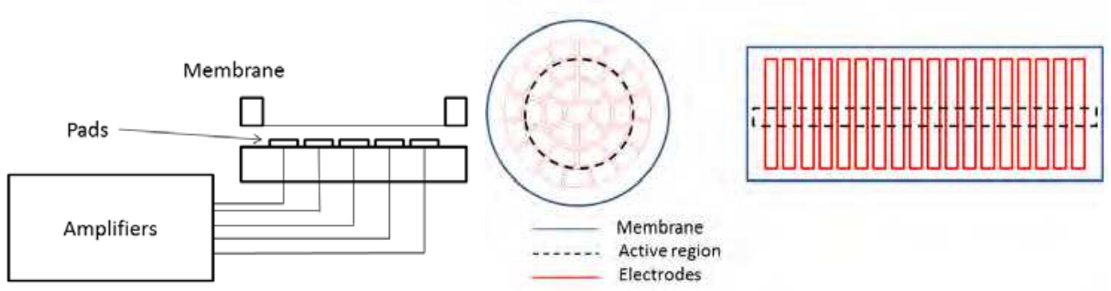

(a) (b)

Fig. 1. Left panel: electrostatic membrane mirror section view. Right panel: membrane active region (delimited by the dashed lines) and actuator footprint; the shown shapes of the actuators are only indicative examples.

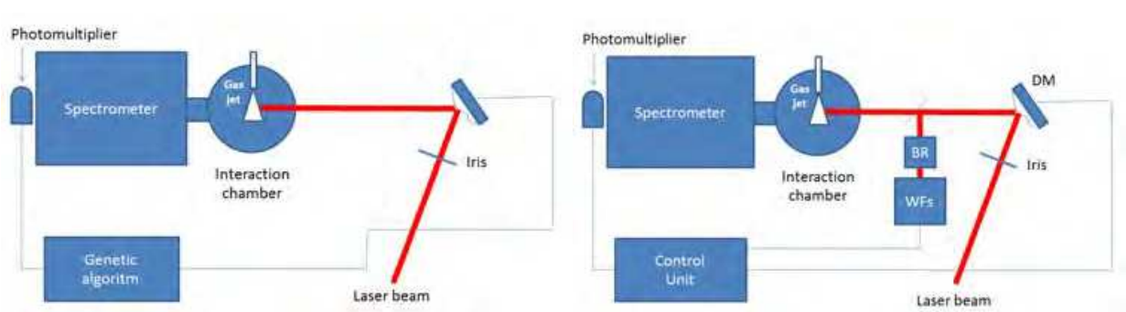

(a) (b)

Fig. 2. (a): schematic of the high order harmonics generation (HHG) experimental setup with sensorless AO system. (b): schematic of the HHG experimental setup for wavefront sensor (WS) AO closed loop system. DM, Deformable Mirror; BR, Beam Reducer; WFs, Wavefront Sensor.

Another interesting application of membrane DM's has been realized in ultrafast laser pulse compression experiments, through a suitable preliminary characterization of the experimental

setup by means of interferometric measurements. The review of Brida et al. (2010) reports many examples of pulse compression of parametric amplifiers based on spectral phase measurement, using the frequency resolved optical gating technique in different spectral regions. In these experiments, a rectangular membrane DM is used to change the Optical Path Length (OPL) of each spectral component of the parametric source in order to cancel the dispersion and to achieve the shortest laser pulse duration (the so-called transform limited pulse). Fig. 3 illustrates the experimental layout of the adaptive compressor: it is composed of a dispersing element, either a prism or a diffraction grating, followed by a spherical collimating mirror which reflects each colour component in a different position on a rectangular membrane DM. The spectral phase added by the DM to each colour component is given by the formula

$$\Delta\varphi(x) = 2\frac{2\pi}{\lambda(x)}\delta z(x), \tag{1}$$

where $\delta z(x)$ is the membrane displacement in the position x relative to the wavelength $\lambda(x)$.

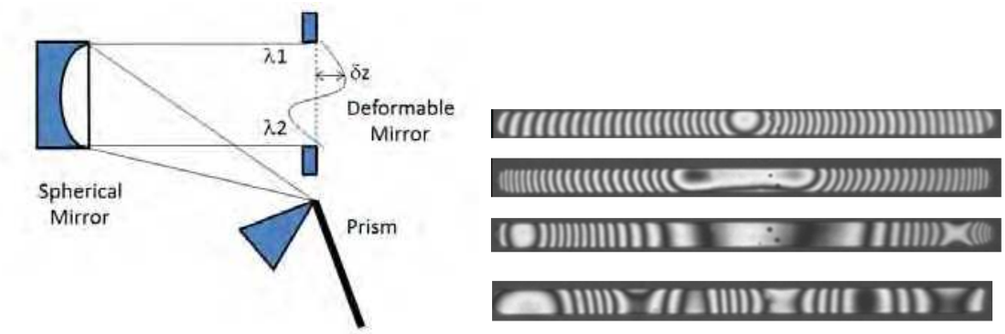

(a) (b)

Fig. 3. (a): 4-*f* arrangement of a prism compressor for femtosecond optical parametric amplifiers. (b): examples of interferograms of the rectangular deformable mirror during the experiment characterization: these interferograms allowed to determine the mirror deformations necessary to optimize the pulse compression.

Another successful application of membrane DM's, where the shape to be given to the DM was known a-priori, and the deformation set to be given to the DM was pre-determined by interferometric measurements, was carried out in quantum optics experiments (Bonato et al., 2006; Bonato et al., 2010). For example, in Ref. (Bonato et al., 2010), a membrane rectangular DM was used for the stabilization of the phase of a two-photon entangled state. The experimental setup (see Fig. 4) consisted in an interferometer in which random fluctuations of the OPL resulted in detrimental fluctuations of the relative phase of the quantum superposition. The membrane DM was used as the optical element able to modulate the relative OPL of the two arms of the interferometer. In order to achieve that goal, two small areas on the linear DM were used as flat plane mirrors whose relative distance could be adjusted. The corresponding DM deformation was obtained thanks to the preliminary determination of the influence functions by means of an interferometer and then by finding the electrode voltages providing the deformations, as shown in Fig. 5. The thick blue lines in this figure represent the two flat mirror areas where the beams are reflected.

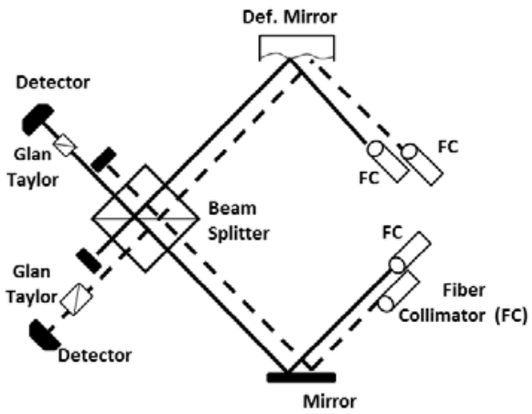

Fig. 4. Experimental apparatus for the quantum interferometer stabilisation.

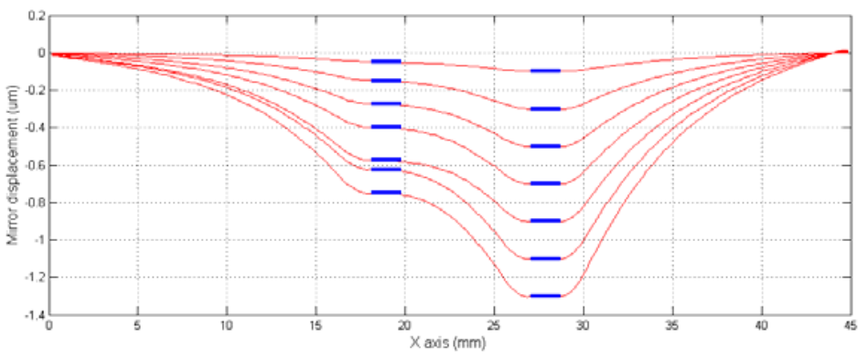

Fig. 5. Measurement of the set of deformations which create a displacements between the blue reference planes.

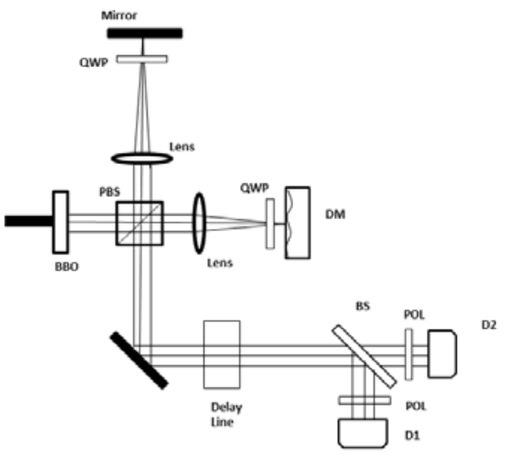

Fig. 6. Hong-Ou_Mandel quantum interferometer which was used to demonstrate the even order aberrations cancellation. The membrane DM is positioned on one arm of a 4-*f* quantum interferometer (BS: beam splitter, QWP: quarter waveplate, BBO: beta barium borate crystal, Pol: polarizer, D: detector).

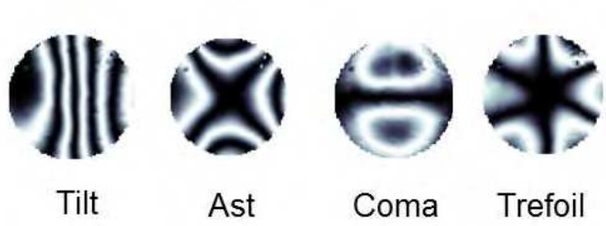

Fig. 7. Measurements of the membrane deformations given by the round membrane DM to demonstrate the even order aberration cancellation.

Another experiment which was carried out by preliminary membrane DM calibration is shown in Fig. 6. This experiment reports on the the first experimental demonstration of the even-order aberration cancellation effect in quantum interference applications. A round membrane DM was used in a 4−*f* AO system to modulate the distribution of wavefronts emitted by a spontaneous parametric down conversion process, so effectively introducing a controllable degree of wavefront aberration. This was used to show that even-order aberrations, such as astigmatism and polynomial (4,4), do not affect the interferograms, and that the quality of the quantum interference only depends on odd-order aberrations (Bonato et al., 2006). Fig. 7 shows the interferometric results of the measurements of the membrane deformations for some of the considered aberrations.

1.2 Membrane deformable mirror control

To control a membrane DM, with either round or rectangular shape, it is necessary to characterize it through the acquisition of the influence function matrix (IFM). Since the electrostatic membrane mirror can just pull the membrane, for allowing the aberration compensation on both directions it is necessary to work biasing the membrane to its middle: with respect to this bias ("starting") position, it is possible to both pull and push the membrane. The IFM can be considered as a basis of linear independent vectors to represent all the possible deformations of a DM. More in detail, given N actuators and a bi-dimensional wavefront domain of rank $M = m_x \times m_y$, the $M \times N$ IFM A is obtained by placing in each column the wavefronts w_1, w_2, ..., w_N, corresponding to the measured wavefronts w_i, a vector of rank M, obtained by activating the i^{th} actuator with a unitary voltage, and called "influence function". By using this definition, and remembering that the electrostatic pressure depends on the square of the applied voltage, it is easy to write any mirror deformation as a linear combination $w = Av$, where v is an M rank vector of the square applied voltages. Fig. 8 shows some examples of influence function interferograms obtained by applying a unitary voltage to the membrane DM's shown in Fig. 1.

In order to know which voltages have to be applied to the actuators to obtain a specific DM deformation, the problem of the IFM inversion has to be solved. This is realized, for example, with the so-called pseudo-inversion standard technique, by means of the Singular Value Decomposition (SVD), as follows. Given the matrix A, it can be factorized as

$$A = U\Sigma V^* , \tag{2}$$

where U is an $m_x \times m_x$ unitary matrix, the $m_x \times m_y$ matrix Σ has non-negative numbers on the diagonal and zeros off the diagonal, and V^* denotes the conjugate transpose of V, an $m_y \times m_y$

unitary matrix. At this point, we can use the rule for which the pseudo-inverse of the matrix A with singular value decomposition $A = U\Sigma V^*$ is:

$$A^+ = V\Sigma^+ U^*, \tag{3}$$

where Σ^+ is the transpose of Σ with every nonzero entry replaced by its reciprocal.

The application of this technique to the specific problem is that given the IFM A of the influence functions, the matrix V represents an orthogonal base composed by the modes of the mirror. The values in the diagonal matrix Σ are the gains of each mode. The gain values are in decreasing order, and the modes are ordered from the lowest spatial frequency to the highest one. Therefore, the larger gain corresponds to the lower spatial frequency mode. Fig. 9 shows the interferograms of the modes for a round membrane DM.

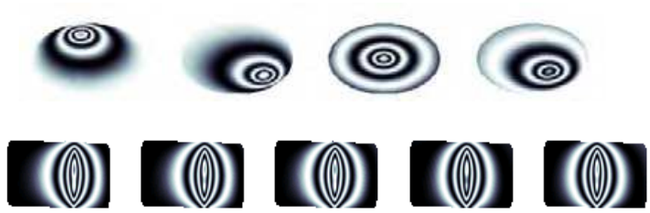

Fig. 8. Examples of interferograms of the influence functions generated by the actuators for a round membrane DM (top) and for a rectangular membrane DM (bottom).

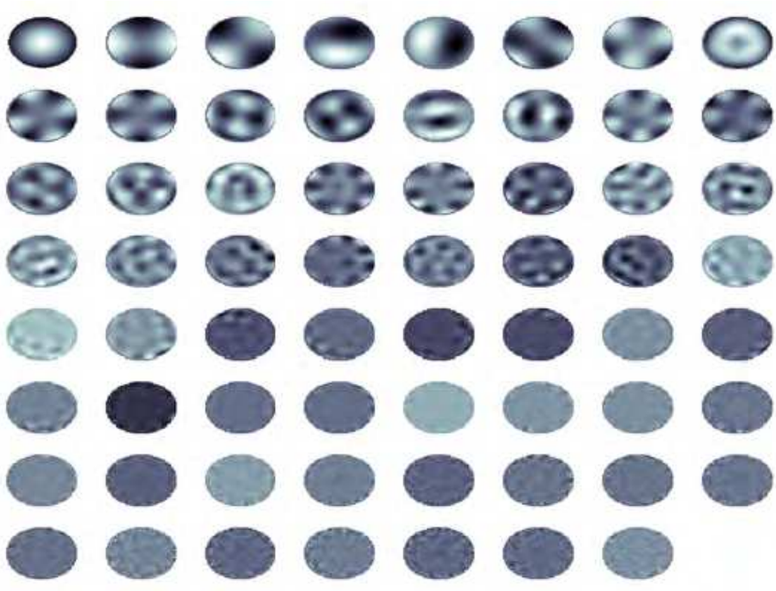

Fig. 9. Modes relative to a 61 electrode membrane DM.

At this point, the fit of the wavefront passes through the determination of the ideal number of necessary modes. Ideally the higher the number of modes the better the reconstruction, because using a high number of modes means to be able to reproduce with better accuracy the high spatial frequency mode. However, in practise there are two main limitations. The first is that the voltage range is usually limited: so, since the high order modes have a small

gain, using a large amount of modes usually makes the algorithm saturating the voltages. The second is the presence of noise: usually noise measurements or artefacts get coupled with the highest orders, driving the algorithm to wrong solutions and to voltage saturation.

Fig. 10 shows the root mean square (RMS) deviation of the generated wavefront from the ideal correction against the number of used modes. It is evident that using just a few modes is not sufficient to fit the solution with enough accuracy, while on the contrary the reconstruction error can be very low if a number of modes between 10 and 22 is used. However, as explained before, it is also clear from this plot that the noise tends to reduce the system performance when a higher number of modes is used. The standard deviation of the voltages with respect to the bias level against the number of used modes is illustrated in Fig. 11 (the maximum voltage with respect to bias is 64 V). Comparing Figures 10 and 11, it is easy to note that after about 20 modes the voltage level increases with a deterioration of the results.

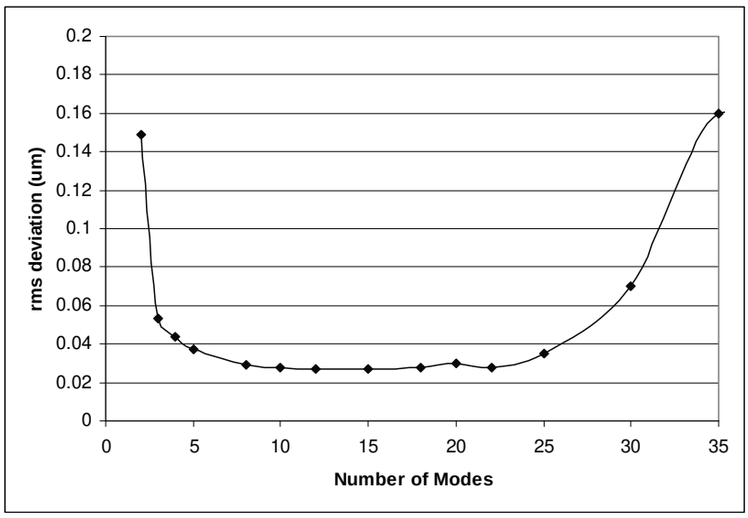

Fig. 10. RMS error in the fit of the solution against the number of modes used.

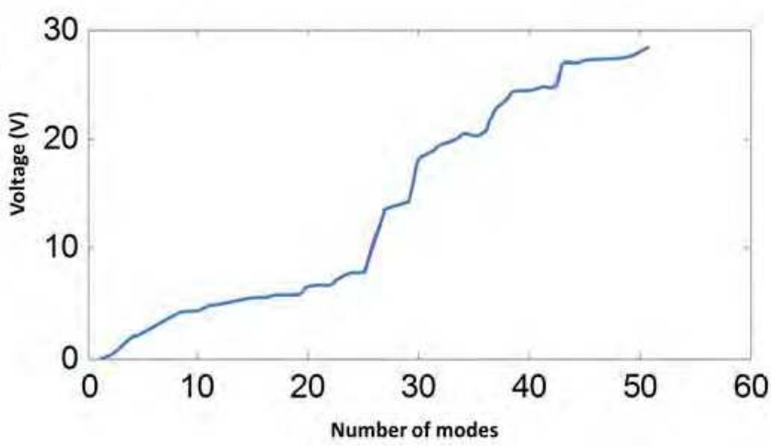

Fig. 11. Standard deviation of the voltage applied to the actuators with respect to the bias level, versus the number of used modes.

2. Resistive actuators deformable mirror for sensorless applications

Sensorless applications play an important role in the AO development thanks to the reduced hardware complexity. With this technique it is possible to improve the image quality or, for example, to increase the efficiency of a laser process affected by aberrations, through the optimization of a specific merit function. The resistive Modal Deformable Mirror (MDM) is an electrostatic membrane DM where the actuators are composed by a resistive layer which continuously distributes the electrostatic pressure on the membrane. An example of actuators layout optimized for the direct generation of aberrations with the minimum number of actuators is illustrated in Fig. 12 (a). Its convenience and flexibility of use have been recently demonstrated in two completely different fields such as visual optics for the optimization of image quality (Bonora, 2011a) and non-linear ultrafast optics for the optimization of the harmonics generation in gases.

The MDM addresses two problems: 1) the use of the smallest possible number of actuators, 2) the introduction of the DM modal control in a continuous actuators arrangement. The main feature of the resistive MDM is that the actuators response is directly related to the optical aberrations allowing for a more versatile and straightforward use than conventional discrete actuators deformable mirrors. In the MDM, the voltages necessary to drive the mirror can be directly computed from the Zernike decomposition terms of the target aberrations, leading to an ideal device for modal control in sensorless applications.

As an example of resistive MDM, we can consider a membrane electrostatic DM composed by a silvered 5 μm thick nitrocellulose membrane suspended 70 μm above the actuators by some spacers. The prototype described in ref. (Bonora, 2011a) mounts a membrane of 19 mm diameter designed for an optimal deformable active region of 10 mm diameter. This prototype is driven by a DM multichannel electronic driver (Adaptica IO32) which can supply up to 260 V over 32 channels; in order to generate both positive and negative deformations, the membrane is connected to a voltage reference of 130 V.

The DM is actuated at the position (x,y) by the electrostatic pressure $p(x,y)$ between the actuators and the metalized membrane which deforms the mirror surface $M(x,y)$ according to the Poisson equation

$$\Delta M(X,y) = \frac{1}{T} p(x,y) \,, \tag{4}$$

where T is the mechanical tension of the membrane.

The device is composed by 3 actuators placed on three concentric rings (see Fig. 12). The actuators are composed by a 35 μm thick graphite layer which presents a sheet resistance of 1 MΩ/inch² which continuously distributes the voltage. The estimated current for each channel when applying the maximum voltage, is about 60 μA with a power consumption for each actuator of about 10 mW.

The voltage distribution over the resistive layer with resistivity ρ can be computed solving the Laplace equation for the scalar electric potential U:

$$\frac{1}{\rho}\Delta U(x,y)=0\,. \tag{5}$$

By a proper design of the MDM, actuator 3 (see Fig. 12(a)) can be used to generate piston, tilt and astigmatism, actuator (2) can be used for the generation of coma and defocus, and actuator 1 for the generation of spherical aberration. In order to solve both formulas (4) and (5) we applied the recursive finite difference method. Fig. 13 reports some examples of simulated voltage distributions, and of the corresponding electrostatic pressure and mirror deformation for each actuator ring.

Following Bonora (2011a), the resistive MDM response can be directly derived from the Zernike decomposition of the incoming wavefront, realizing a modal control of the DM, rather than from the influence functions (zonal control). Thus, the voltages V_{MDM} which generate the aberrations described by the Zernike coefficients are determined by the algebraic sum of the voltages which generate each single aberration defocus, astigmatism, coma and spherical aberration:

$$V_{MDM}=V_{defocus}+V_{astigmatism}+V_{coma}+V_{spherical}\,. \tag{6}$$

By using (6), it is possible to generate any aberration starting from the knowledge of its Zernike spectrum.

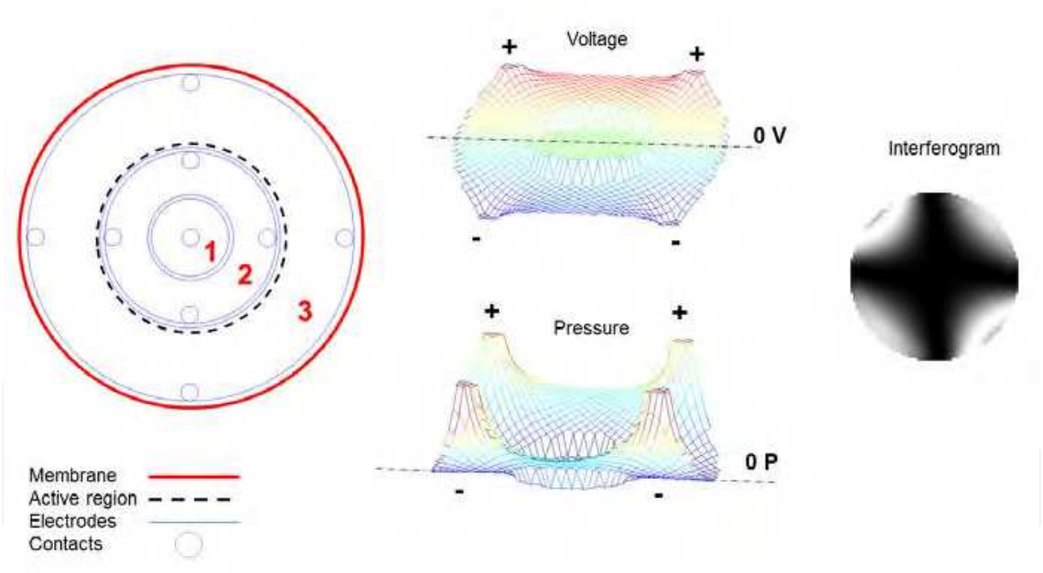

(a) (b) (c)

Fig. 12. (a): Layout of the electrodes of the resistive MDM. The two external ring actuators, number 2 and 3, have four symmetrical electrical contacts each, while the central one, number 1, has a single central electrode. (b): voltage distribution and relative induced electrostatic pressure generating an astigmatic mirror deformation. (c): interferogram of the MDM surface deformed by the electrostatic pressure shown in (b). The application of both positive and negative voltages generates a zero voltage distribution (dotted line 0 V) in the middle of the membrane which corresponds to a zero electrostatic pressure (dotted line 0 P).

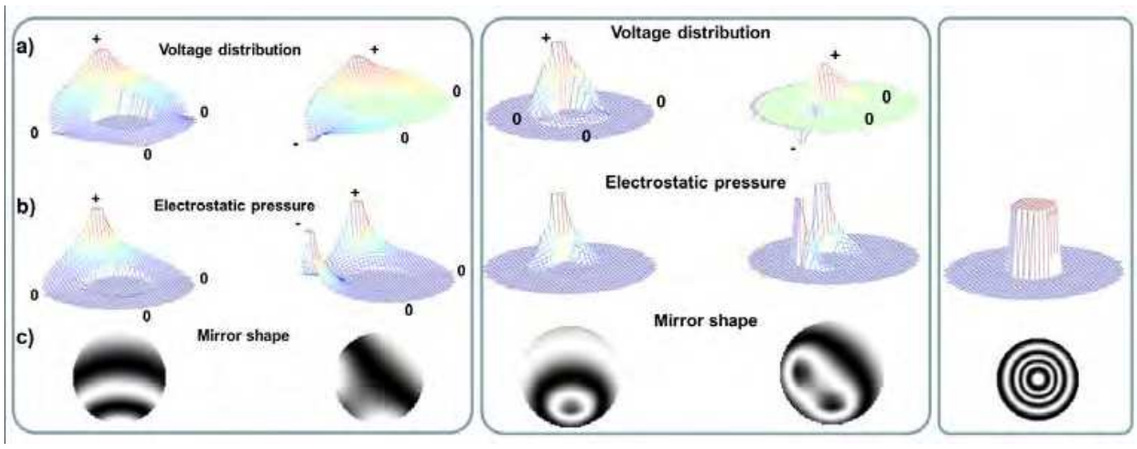

Fig. 13. Simulation results. Left box: examples of voltage distribution (top), electrostatic pressure (middle) and membrane shape (bottom) using the outer ring. Central box: as for the left box, using the central actuator ring only. Right box: as for the previous, applying voltage only to the central actuator.

2.1 Control algorithm

The properties of the MDM allow to use a sequential aberration correction algorithm, that is an algorithm which allows to correct each single aberration in a sequence, as illustrated by the block diagram of Fig. 14. As reported by Debarre & Booth, 2007, image sharpening functions related to low frequencies can be expanded as the quadratic sum of the aberration coefficients. Exploiting this property, it is possible to see that the aberration correction: a) can be operated by the maximisation of the sharpening function of each single aberration; b) is independent of the order of the optimization sequence; c) can be resolved by three single measurements. The optimization strategy starts with the optimization of a merit function applying a defocus to the MDM; then, fixed the best defocus value, the optimization is carried out to astigmatism, then to spherical aberration and finally to coma. This algorithm has been applied successfully in visual optics (see section 2.3.2) and laser focalisation experiments (see section 2.3.3).

2.2 Examples of application of the resistive modal deformable mirror

2.2.1 Application of resistive MDM for eye aberration correction

To evaluate the performance of a resistive MDM for the compensation of ocular aberrations, we used the above established principles, as reported by Thibos et al. (2002). To have a better idea about the actual potentialities of the MDM, a comparison of its correction performance has been realized with a commercially available 32-actuator electrostatic membrane DM (Pan DM, Adaptica srl) (Bonora et al., 2006a). The actuator layout of the two DM's is shown in Fig. 15.

The performance comparison has been realized by analysing the DM's maximum stroke necessary to correct a sample eye population with the same average residual. The results reported in Fig. 16 show the RMS wavefront deviation before and after correction, for a population of 50 eyes. From this comparison, it can be noticed that the resistive MDM is equivalent to the commercial Pan DM with a stroke reduced by 25%.

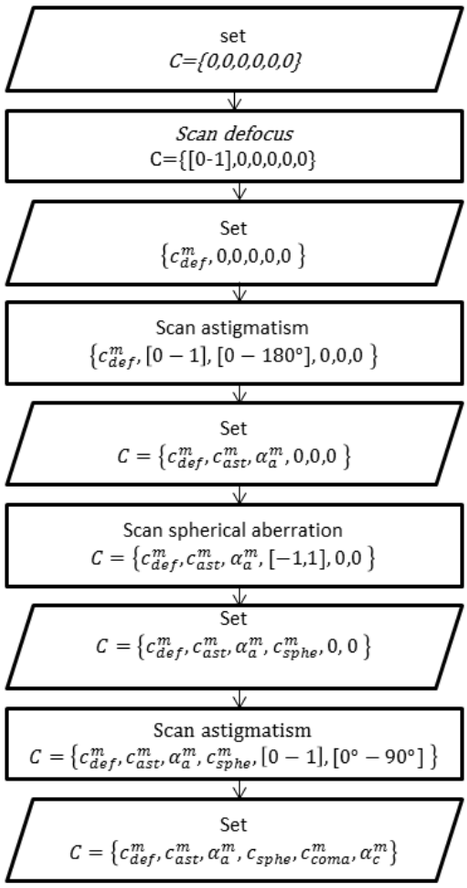

Fig. 14. Block diagram showing the sequence of the aberration correction algorithm implemented on the MDM.

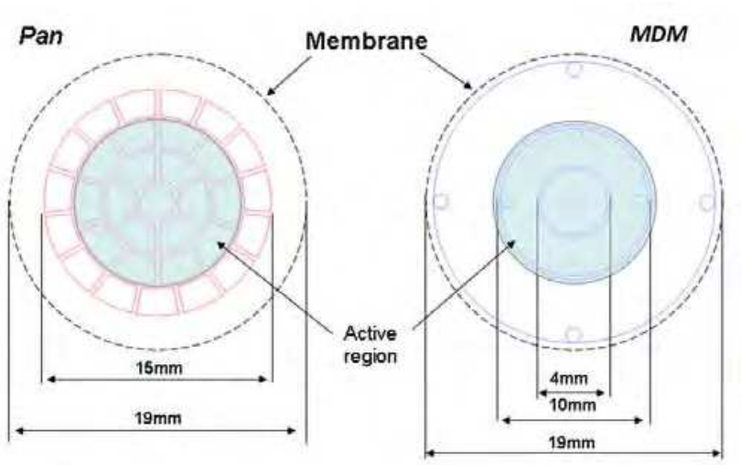

Fig. 15. Actuator layout for both the commercial Pan DM (left) and the resistive MDM (right).

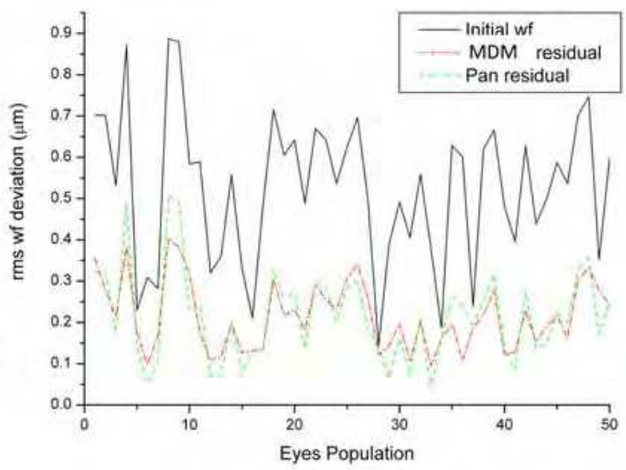

Fig. 16. RMS wavefront deviation for the aberrations of a sample of 50 eyes before and after DM correction. The two DM's under test are a resistive MDM and a commercial discrete electrodes DM.

2.2.2 Visual optics application of resistive MDM

An experiment of sensorless optimization using a resistive MDM is reported by Bonora, 2011. In this experiment, a sample image (a honeybee leg) has been altered by the introduction of an aberrated phase plate. The result is a degradation of the image quality as shown in Fig. 17: the top row shows an interferogram, the image and the Point Spread Function (PSF) after the introduction of the aberrated phase plate and defocus correction; the bottom row shows the same optical parameters at the end of the correction, realized through a 30 acquisition process.

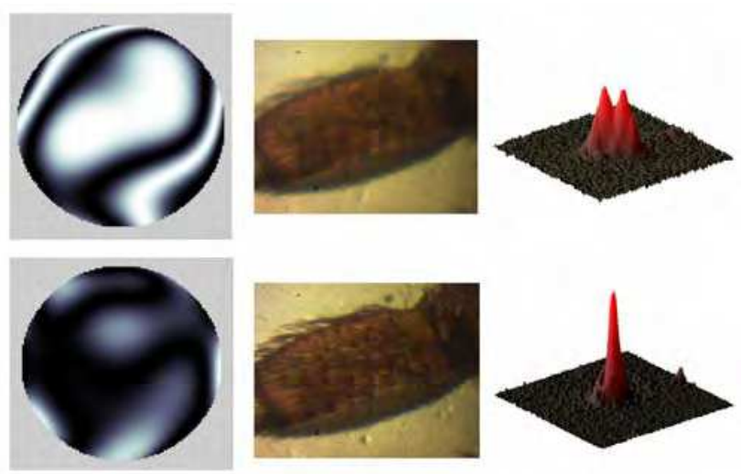

(a) (b) (c)

Fig. 17. Improvement of the quality of an aberrated honeybee leg image by the use of a resistive MDM. The top row corresponds to the situation after the defocus correction, while the bottom one corresponds to the status at the end of the correction process. Column (a) shows the interferograms of a central image point; column (b) shows the images; column (c) shows the PSF at the center of the field.

As can be clearly seen, by the application of the low spatial frequency image sharpening function and of the algorithm described in Fig. 14, it has been possible to largely increase the image quality, with a significant reduction of the image aberrations.

Fig. 18 shows the evolution of the selected merit function during the scan of the defocus, astigmatism, spherical aberration, and coma performed during the correction process. Each scan was carried out with 5 acquisitions and interpolated with a polynomial curve to find the aberration value which maximizes the merit function.

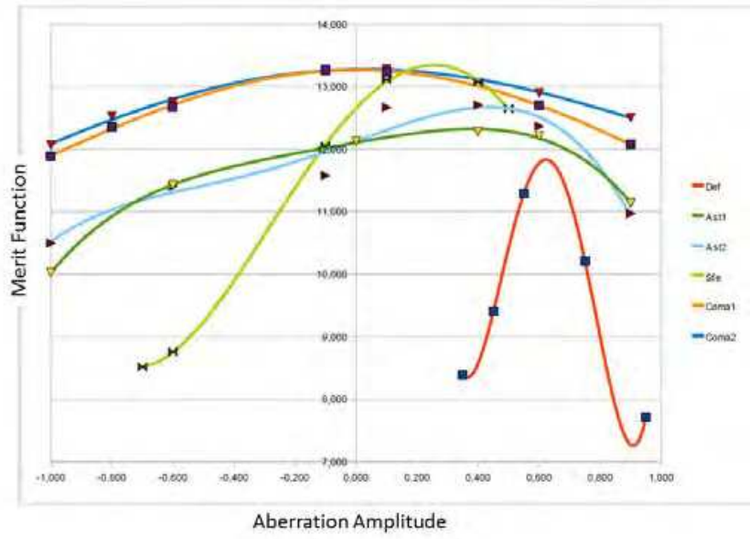

Fig. 18. Evolution of the merit function during the scan of the defocus, astigmatism, spherical aberration, and coma during the correction process.

2.2.3 Resistive MDM for laser focalisation application

Another interesting application of a resistive MDM was carried out to optimize the harmonic generation from the interaction of a tunable high energy mid-IR optical parametric amplifier (OPA) with a krypton gas jet (Vozzi at al., 2007, Bonora et al., 2011b). In this case, a fast sensorless optimisation system is the key for the aberration correction: in fact, the alternative solution with a mid-IR WS is possible but at the price of a higher cost and an increase of the experimental complexity; moreover, the relatively low repetition rate of the amplified systems effectively results in the practical impossibility of using other algorithms, as for example the random search one, which needs hundreds of iterations.

The experimental setup used for this application is illustrated in Fig. 19. To demonstrate the easiness of implementation of this device within the experiment, the optical path before the DM is shown with a dotted line. The additional elements are simply a plane mirror and the resistive MDM, which have been introduced without complex operations. The obtained system optimization consisted in an increase of the harmonic signal detected by the photomultiplier at the output of the monochromator. This result is illustrated in Fig. 20, where it is possible to see that the photon flux on the photomultiplier is doubled with respect to the one obtained after the defocus correction.

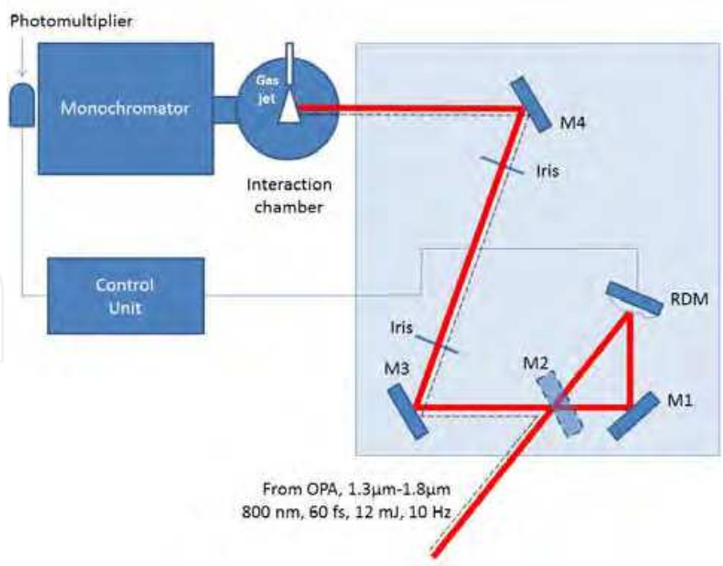

Fig. 19. Experimental setup for the generation of harmonic from a femtosecond tunable high energy mid-IR OPA. Dotted line: optical path before the experiment with the MDM. Red line: optical path realized for the experiment with the deformable mirror.

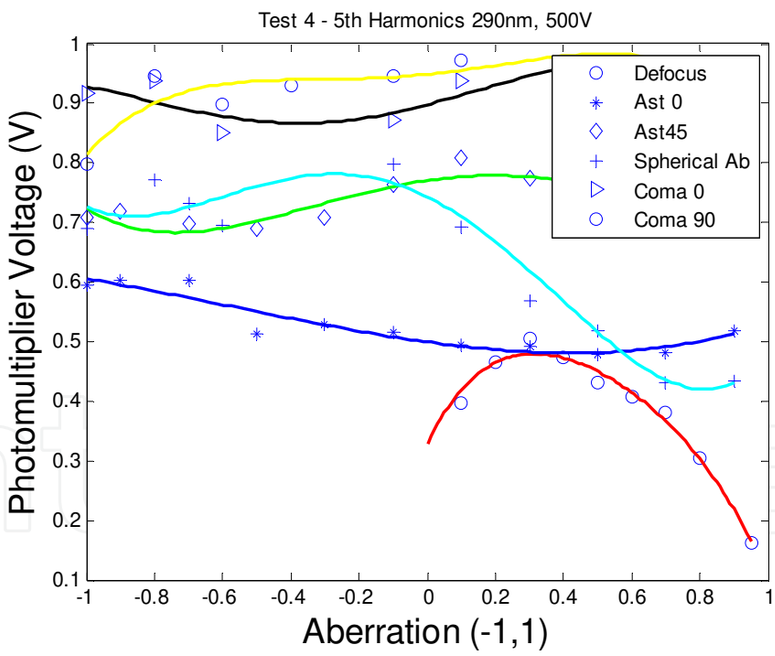

Fig. 20. Optimization of the voltage generated by the photomultiplier over a 50 Ω load for the 5th harmonic at 290 nm, obtained by the use of krypton gas.

3. Push-pull membrane deformable mirror

Membrane DM's are rather diffused thanks to their simplicity, low cost and the bipolarity of the reproduced deformation that allows closed loop operations without biasing. A

disadvantage which can be encountered when using membrane DM's is the not so large amount of stroke that is possible to achieve, and that in some cases can limit the instrument performance. A solution to overcome this problem has been found realizing membrane DM's with electrodes positioned both on the bottom and on the top of the membrane. Using this layout the membrane can be pulled on both sides, thus increasing the optical power of the DM. Prototypes of push-pull membrane electrostatic mirror have been realized for visual optics applications using a transparent front electrode (Bonora & Poletto, 2006), while another prototype for pulse compression and shaping has been realized in a square shape with a central slit to get the light onto the membrane (Bonora et al., 2006b).

Fig. 21 shows the schematic layout of a push-pull membrane DM. In this DM, the top-side electrodes are realized with an Indium-Tin-Oxide (ITO) coating, which is transparent to visible light and electrically conductive, deposited on a front disc glass, whereas the back electrodes are printed on a standard electronics Printed Circuit Board (PCB). A sketch of the electrode patterns is depicted in Fig. 22. As demonstrated in Vdovin et al., 2006, a membrane DM is more effective when outside the active area there is at least one ring of actuators. For this reason the active region of this DM corresponds to the glass window in the front side actuators. Some examples of electrodes deformations are given in Fig. 22 for both the front and the back side electrodes.

To generate controlled large mirror deformations with push-pull membrane DM's, Bonora & Poletto, 2006 reports an interesting algorithm which exploits electrodes saturation (see block diagram in Fig. 23). In this algorithm, the electrostatic pressure p, which induces the membrane shape, is initially calculated by the pseudoinversion of the influence functions matrix A starting with the target shape Z; then all the electrode voltages that should nominally be above the saturation threshold are fixed to the saturation value, and all the others are iteratively used to decrease the membrane shape residual. A comparison between the pull-only electrostatic DM and the push-pull electrostatic DM implementing this algorithm has been carried out for the aberrations up to the 4^{th} order: as illustrated in Fig. 24, the push-pull DM demonstrated to have nearly twice the optical power than the pull-only DM.

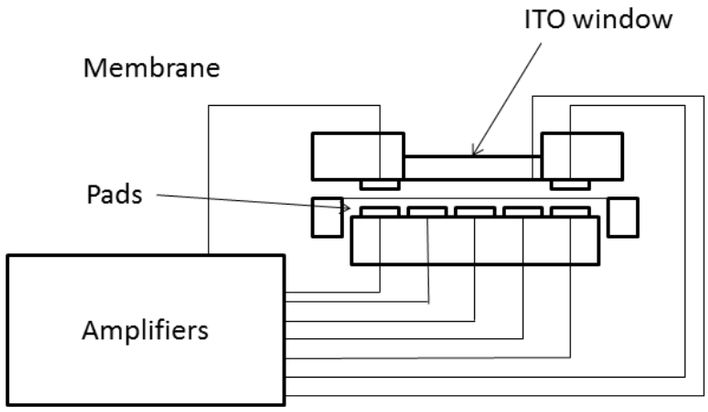

Fig. 21. Schematic layout of a push-pull DM cross section.

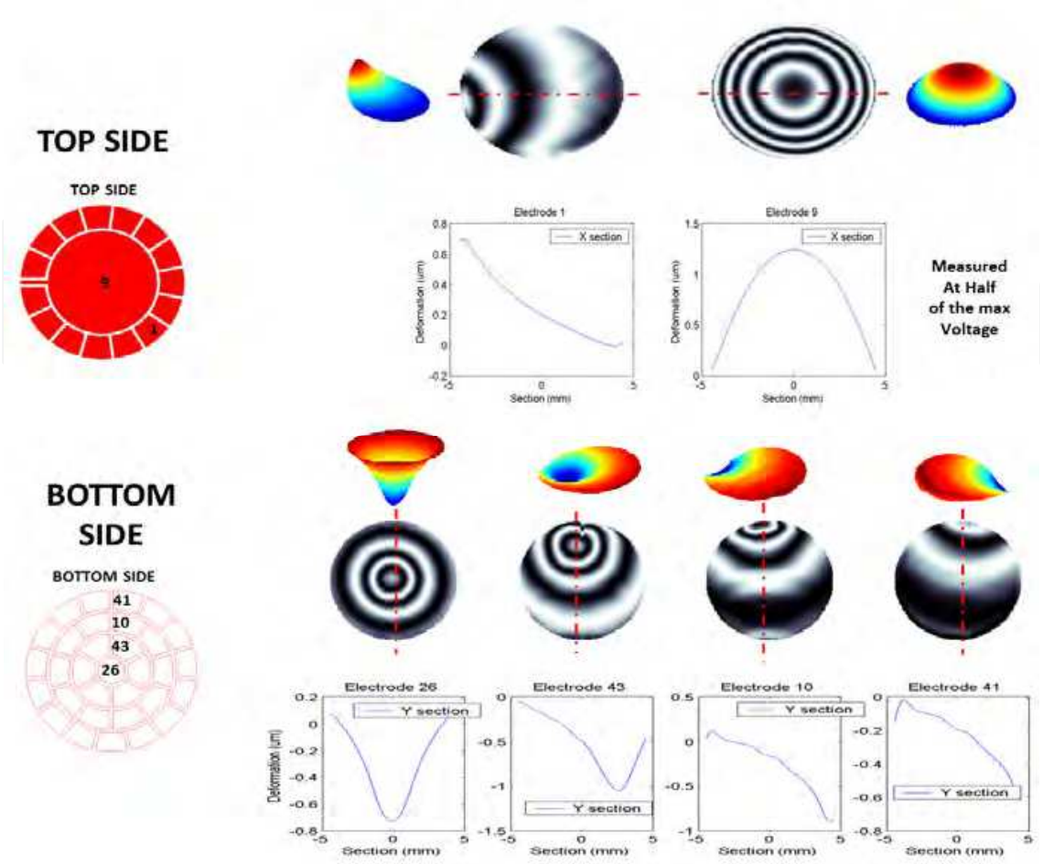

Fig. 22. Front side and back side electrodes footprint (left) and influence functions (right).

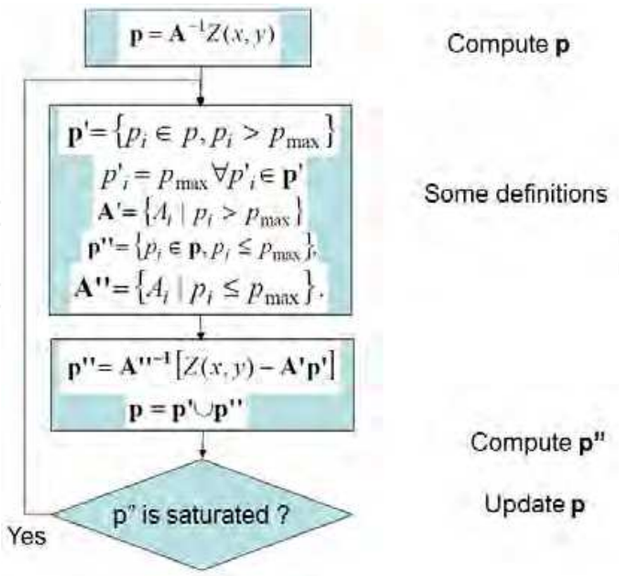

Fig. 23. Block diagram for the exploitation of the saturation in the calculation of the electrostatic pressure "*p*". *A* is the influence functions matrix, and *Z*(*x*,*y*) is the aberration target.

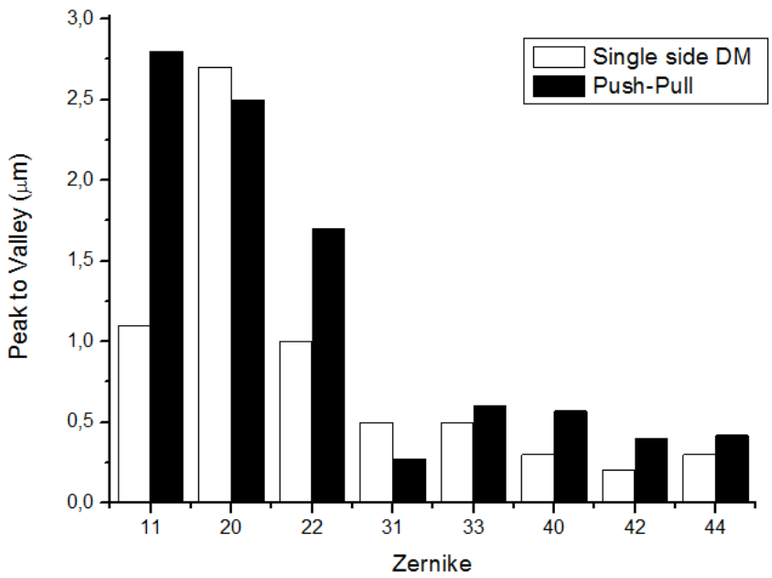

Fig. 24. Comparison between the pull-only and the push-pull membrane DM's in the generation of Zernike polynomials.

3.1 An application of the push-pull membrane DM

Push-pull linear membrane DM's have been found an interesting application in femtosecond parametric amplifiers compression and shaping (Weiner, 2000). In fact, as reported by Brida et al., 2010, using DM's is the optimal way to manipulate the broadband radiation coming from an ultrabroadband OPA: it has been shown (see for example Zeek et al., 1999, Brida et al., 2010) that the use of a DM as spectral phase modulator has significant advantages with respect to acousto-optics modulators and liquid crystals, as for example high efficiency and achromaticity, at the expenses of a slightly smaller resolution.

The pulses produced by ultrabroadband OPA with the linear membrane DM's have found many important scientific applications in material science to study physical phenomena which happen on the femtosecond timescale, such as for example the study of the quantum dynamics of photoelectrons in Mott insulators (Wall et al., 2001). Unfortunately the limited stroke of the used membrane DM's allowed just to realize pulse compression and not also pulse shaping. The recent use of push-pull membrane linear DM's (Brida et al., 2010) sorted this limit out, demonstrating that also pulse shaping can be obtained with a push-pull DM. The device layout is illustrated in Fig. 25: the back side electrodes are rectangular and fill the whole membrane area, while the front electrodes have a small slit in the centre to allow the OPA light to reach the reflective membrane.

Using this push-pull DM, it was demonstrated that it is possible both to compress ultrabroadband pulses and to shape their temporal profile. Couples of 20 fs pulses with temporal separation tunable between 0 to 150 fs have been measured and used to control the dynamics of LD690 dye molecules.

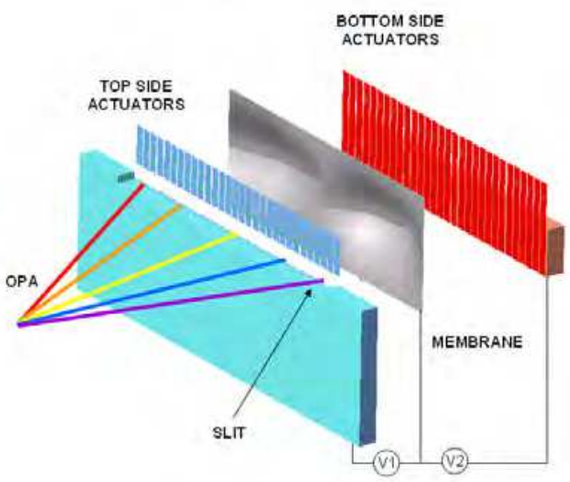

Fig. 25. Layout of the push-pull deformable mirror for pulse shaping with OPA.

4. Photo-controlled deformable membrane mirror

A new type of membrane DM is made by associating a metalized membrane with a monolithic non-pixelated photoconductive substrate (Bortolozzo et al., 2010). The assembly constitutes a continuous photo-controlled deformable mirror (PCDM), which is driven by sending suitable light intensity distributions onto its photoconductive side, opposite to the reflection side. This approach, eliminating the spatial segmentation of the driving elements, provides a continuous photo-addressing of the mirror and thus largely simplifies the driving electronics; in addition, at the same time, it allows to realize more flexible configurations.

As an example, a PCDM made by using a photorefractive $Bi_{12}SiO_{20}$ (BSO) crystal as a photosensitive element is depicted in Fig. 26. The BSO is cut in the form of a thin disk, 1 mm thickness and 35 mm diameter, coated on one side with an Indium-Tin-Oxide (ITO) transparent electrode; the facing membrane is a nitrocellulose layer, 19 mm diameter and 5 μm thickness, metalized by an Ag coating and mounted on a rigid aluminum ring. Mylar spacers are introduced between the BSO and the ring supporting the membrane, in order to provide a gap of a few tens of microns. When an ac voltage is applied to the PCDM, the electrostatic pressure across the gap attracts the membrane towards the BSO substrate. Since the impedance of the BSO decreases with the light intensity, when the BSO is uniformly illuminated a large deformation in the form of a paraboloid is induced on the membrane. Once the membrane has reached an equilibrium position, further deformations can be superimposed by local point-like illuminations of the BSO. PCDM with gaps of 50 μm were realized as a good compromise between the optimization of the capacitive effect and the maximum allowable deformation before the membrane snaps down on the photoconductive substrate. The membrane deformation was measured by using a visual interferometric profilometer (Zygo GP-LC). When the voltage is applied across the mirror, the membrane deformation is directly seen as a radial displacement of the fringe pattern.

From the measured phase change $\Delta\varphi$, the maximum membrane deformation Δx can be derived as:

$$\Delta\varphi = \frac{2\pi}{\lambda} 2\Delta x \,, \tag{7}$$

where λ is the optical wavelength. Uniform illumination of the BSO side with an expanded laser beam at 474 nm wavelength, which is inside the range of maximum response of the BSO (Gunter & Huignard, 2006), leads to membrane deformation of the order of a few microns. The maximum deformation Δx is plotted in Fig. 27 both as a function of the light intensity I_{PC} on the BSO side at different amplitudes of the applied voltage V_o, and as a function of the operating frequency f.

The model accounting for the equilibrium deformation of the membrane is derived by considering that the membrane deformation $M(\rho,\theta)$ obeys a Laplace equation

$$\nabla^2 M(\rho,\theta) = \frac{\varepsilon_o}{2T} \frac{V_{GAP}^2}{d^2} \,, \tag{8}$$

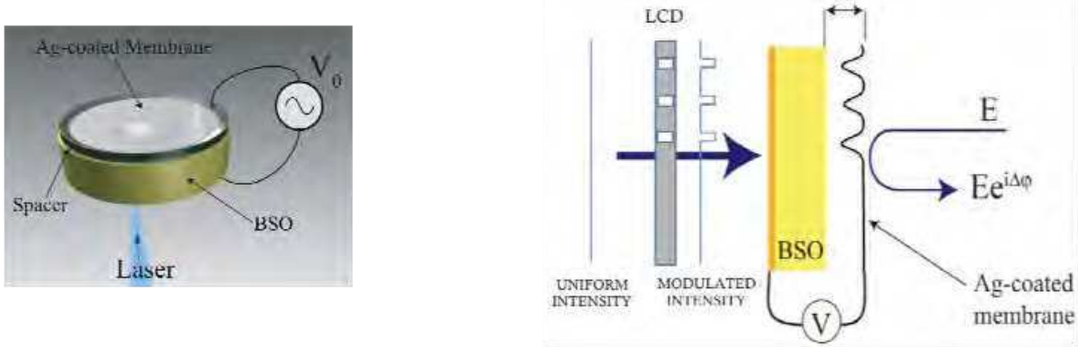

(a) (b)

Fig. 26. (a): Schematic representation of a photocontrolled deformable membrane mirror. (b): selective optical addressing by the use of a liquid crystal display (LCD); the membrane deformation follows the intensity distribution on the BSO and the reflected beam acquires a correspondent phase shift $\Delta\varphi$.

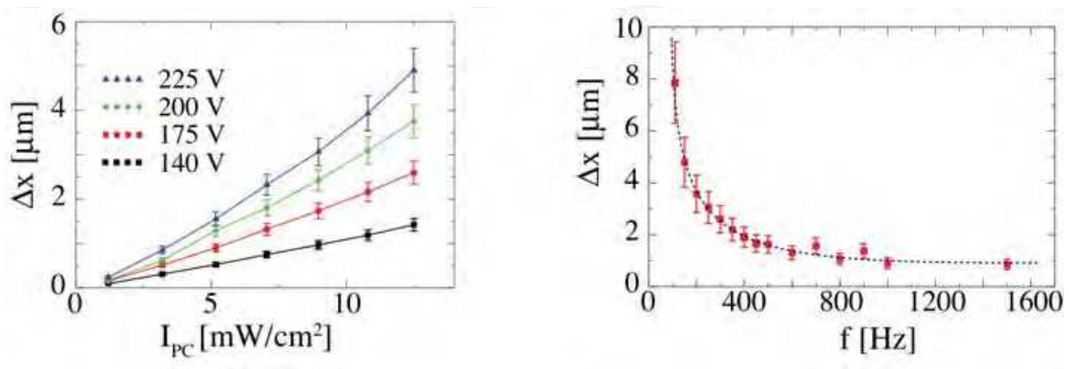

(a) (b)

Fig. 27. (a): Membrane maximum deformation Δx as a function of the light intensity I_{PC} on the photoconductor side of the mirror; f = 1 kHz. (b): membrane maximum deformation Δx as a function of the frequency f of the applied voltage; V_o = 140 V peak-to-peak.

where ρ and θ are the radial and angular directions, respectively, T is the membrane tension factor, V_{GAP} is the effective voltage that drops across the empty gap of the mirror and d is the thickness of the gap. By approximating the membrane deformation with a parabolic profile, and by taking the appropriate boundary conditions, we obtain that the maximum membrane deflection $M(0,\theta) \equiv \Delta x$ occurs at the center, $\rho = 0$, and is given by

$$\Delta x = \frac{\varepsilon_o}{32T}\frac{a^2 V_{GAP}^2}{d^2}, \tag{9}$$

where a is the diameter of the membrane (Efron & Dekker, 1995). By approximating the BSO response with a linear function (Bortolozzo & Residori, 2006), we have that $V_{GAP} = \Gamma V_o + aI_{PC}$, where V_o is the voltage externally applied to the mirror, Γ the dark impedance of the BSO, I_{PC} the intensity of the photo-addressing beam and α a phenomenological parameter that can be deduced from the mirror characteristics. By developing Δx at the first order approximation, we obtain

$$\Delta x = \frac{\varepsilon_o}{32T}\frac{a^2\Gamma^2 V_o^2}{d^2}\left(1 + 2\frac{\alpha I_{PC}}{\Gamma V_o}\right). \tag{10}$$

Since the phase delay acquired by the probe beam is proportional to Δx, it can be seen from equation (10) that the PCDM provides a phase shift scaling quadratically with V_o and linearly with I_{PC}. For low I_{PC} intensities and for small applied voltages V_o, the linear dependence of Δx from I_{PC} is in agreement with the experimental results (see Fig. 27). When I_{PC} and V_o increase, higher order corrections can take into account the deviations from the linear behavior.

To characterize the spatial resolution, the photoconductive substrate has been addressed by a 474 nm wavelength laser beam with a diameter of 300 µm and intensity $I = 1$ mW/cm². The corresponding local deformation of the membrane is shown in Fig. 28 for three different positions of the photo-addressing beam with respect to the centre of the membrane, $r_1 = 0.05$ mm, $r_2 = 4$ and $r_3 = 6$ mm, respectively. We notice that the membrane rigidity imposes smaller deformations when approaching the boundary.

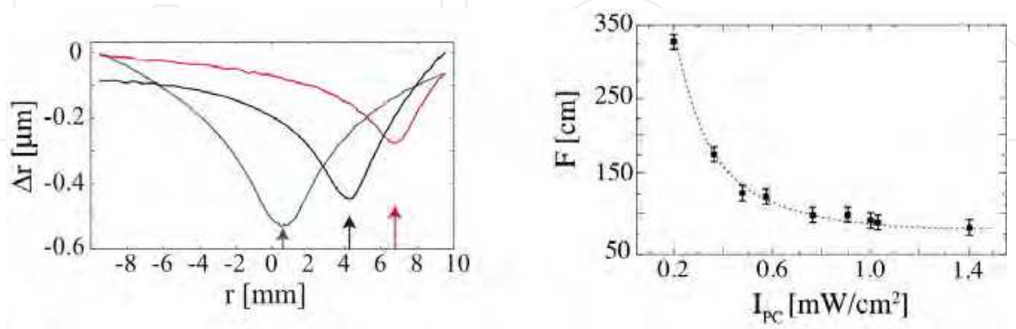

(a) (b)

Fig. 28. (a): Membrane deformation Δr as a response to a light spot illuminating the BSO at different distances from the membrane center; $V_o = 165$ V peak-to-peak, and $f = 400$ Hz. (b): focal length F measured for the reflected beam versus I_{PC} light intensity on the BSO side.

When a localized light spot is sent on the BSO, correspondingly the beam reflected by the membrane is focused at a distance changing with the intensity of the addressing beam. In the right panel of Fig. 28, the measured focal distance F is reported as a function of the addressing intensity, for f = 200 Hz and V_o = 210 V peak-to-peak. A large control of the focal distance is achieved, with F changing from 50 to 350 cm. Other ranges of the focusing distance can be obtained by changing the working point of the PCDM, that is, for other values of f and V_o.

Finally, the performance of the mirror for adaptive optics operations have also been tested. Different target images, corresponding to the Zernike polynomials of the most common mode deformations, have been projected on the photoconductive side of the mirror via a liquid crystal display (LCD). A set of example results is shown in Fig. 29, where the intensity distributions of the beam reflected by the membrane (top row) are shown together with the target patterns (middle), and the corresponding intensity distributions on the BSO (bottom). A very good agreement with the target deformation can be appreciated from the membrane deformation patterns.

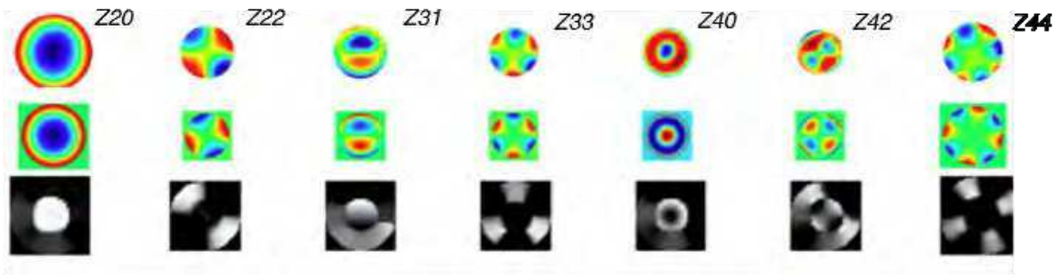

Fig. 29. Example of Zernike polynomial terms generated by the photo-controlled deformable membrane mirror. Top row: membrane deformation; middle row: target deformation; bottom row: corresponding intensity distribution on the photoconductive layer.

5. Conclusions

In this paper we have described some recent technological developments and applications of membrane deformable mirrors. These devices are becoming extremely popular because of their good performance, potentiality, easiness of use, and convenient price.

The described realization technologies and the shown applications of membrane deformable mirrors demonstrate that these adaptive optics devices are presently having a large development activity, with a lot of innovations, with always increasing performance, and with a larger and larger field of applications. All these considerations induce to foresee a rapid extension of the use of membrane deformable mirrors, possibly also in more diffused and commercial applications.

6. References

Bartels R., Backus S., Zeek E., Misoguti L., Vdovin G., Christov I. P., Murnane M. M., Kapteyn H. C., (2000), Shaped-pulse optimization of coherent emission of high-harmonic soft x-rays, Nature, Vol. 406, No. 6792, pp. 164–166, (July 2000), 0028-0836.

Bifano T. (2011), Adaptive Imaging: MEMS deformable mirrors, Nature Photonics, Vol. 5, (2011), pp. 21-23, 1749-4885

Bonato C., Sergienko a., Bonora S., Villoresi P., (2008), Even-order aberration cancellation in quantum interferometry, Physical Review Letters, Vol. 101, No. 23, (December 2008), pp. 233603

Bonato C., Bonora S., Chiuri A.& Mataloni P.& Milani G.& Vallone G.& Villoresi P. (2010), Phase control of a path-entangled photon state by a deformable membrane mirror, JOSA B, Vol. 27, No. 6, (2010), pp. A175-A180, 40-3224

Bonora S., Capraro I., Poletto L., Romanin M.,, Trestino C., Villoresi P. (2006), Fast wavefront active control by a simple DSP-Driven deformable mirror, Review of Scientific Instruments Vol. 77, No. 9, (September 2006), 0034-6748

Bonora S., Poletto L. (2006), Push-pull membrane mirrors for adaptive optics, Optics Express, Vol. 14, No. 25, (December 2006), pp. 11935-11944, 1094-4087

Bonora S., Brida D., Villoresi P., Cerullo G., (2010) Ultrabroadband pulse shaping with a push-pull deformable mirror, Optics Express, Vol. 18, No. 22, pp. 23147-23152, (October 2010), 1094-4087

Bonora S. (2011), Distributed actuators deformable mirror for adaptive optics, Optics Communications, Vol. 284, No. 13, (June 2011), 0030-4018

Bonora S., Frassetto F., Coraggia S., Coreno M., Negro M., Devetta M., Vozzi C., Stagira S., Poletto L. (2011), Optimization of low-order harmonic generation by exploitation of a resistive deformable mirror, Applied Physics B, In press, DOI 10.1007/s00340-011-4820-9

Bortolozzo U., Bonora S., Huignard J.P., Residori S. (2010), Continuous photocontrolled deformable membrane mirror, Applied Physics Letters, Vol. 96, No.25, (January 2010), 0003-6951

Bortolozzo U, Residori S. (2006), Storage of Localized Structure Matrices in Nematic Liquid Crystals, Physical Review Letters, Vol. 96, 037801 (January 2006), 0031-9007

Brida D., Manzoni C., Cirmi G., Marangoni M.,, Bonora S., Villoresi P., De Silvestri S., Cerullo G., (2010), Few-optical-cycle pulses tunable from the visible to the mid-infrared by optical parametric amplifiers, Journal of Optics, Vol. 12, No. 1, (January 2010), 2040-8978

Dalimier E., Dainty C. (2005), Comparative analysis of deformable mirrors for ocular adaptive optics, Optics Express, Vol. 13, No. 11, (May 2005), pp. 4275–4285, 1094-4087

Debarre D., Booth M.J., Wilson T. (2007), Image based adaptive optics through optimisation of low spatial frequencies, Optics Express, Vol. 15, No. 13, (2007), pp. (8176-8190), 1094-4087

Efron U., Dekker M. (1995),Spatial Light Modulators: Materials, Devices, and Systems (Marcel Dekker, New York, 1995)

Grisan E., Frassetto F., Da Deppo V., Naletto G., Ruggeri A. (2007), No wavefront sensor adaptive optics system for compensation of primary aberrations by software analysis of a point source image. Part I: methods, Applied Optics, Vol. 46, No. 25, (2007), pp. 6434-6441, 0003-6935

Günter P., Huignard J.P. (2006), Photorefractive Materials and Their Applications, (Springer, New York, 2006), Vol. 1.

Hardy J.W., 1998, Adaptive Optics for Astronomical Telescopes, Oxford University Press, ISBN-10: 0195090195, USA

Judson R.S., Rabitz H. (1992), Teching lasers to control molecules, Physical Review Letters, Vol. 68, No. 10, (March 1992), pp. (1500-1503), 1079-7114

Naletto G., Frassetto F., Codogno N., Grisan E., Bonora S., Da Deppo V., Ruggeri A. (2007), No wavefront sensor adaptive optics system for compensation of primary aberrations by software analysis of a point source image, Part II: tests, Applied Optics Vol. 46, No. 25, (2007), pp. 6427-643, 0003-6935

Rueckel M., Mack-Bucher J.A., Denk W. (2006), Adaptive wavefront correction in two-photon microscopy using coherence-gated wavefront sensing, PNAS, Vol. 103 , No. 46, (November 2006), pp. (17137-17142), 0027-8424

Thibos L.N., Bradley A., Hong X. (2002), A statistical model of the aberration structure of normal, well-corrected eyes, Ophthalmic, Physiological Optics, Vol. 22, No. 5, (2002), pp. (427-33), 1475-1313

Tyson R., 1999, Adaptive Optics Engineering Handbook , CRC Press, ISBN-10: 0824782755, New York USA

Vdovin G., Soloviev O., Samokhin A., Loktev M. (2008), Correction of low order aberrations using continuous deformable mirrors, Optics Express, Vol. 16, No. 5, (2008), pp. (2859-2866), 1094-4087

Villoresi P., Bonora S., Pascolini M., Poletto L., Tondello G., Vozzi C., Nisoli M., Sansone G., Stagira S., De Silvestri S. (2004), Optimization of high-order-harmonic generation by adaptive control of sub-10 fs pulse wavefront, Optics Letters, Vol. 29, No.2, pp. (207-209), (January 2004), 0146-9592

Vozzi C.& Calegari F., Benedetti E., Gasilov S., Sansone G.& Cerullo, G. Nisoli M., De Silvestri S., Stagira S. (2007), Millijoule-level phase-stabilized few-optical-cycle infrared parametric source, Optics Letters, Vol. 32, No. 20, (2007), pp. 2957-2959, 0146-9592

Wall S., Brida D., Clark S. R., Ehrke, H.P., Jaksch, D., Ardavan, A., Bonora S., Uemura H., Takahashi Y., Hasegawa T., Okamoto H., Cerullo, G., Cavalleri, A. (2011), Nature Materials, Vol. 7, No. 2, (February 2011), pp. (114-118), 1745-2473

Weiner A., Femtosecond pulse shaping using spatial light modulators, Review of Scientific Instruments (2000), Vol. 71, No. 5, (2000) pp.(1929-1962) , 0034-6748

Wright J.& Poland S. P., Girkin J. M., Freudiger C. W., Evans C. L., Xie X. S. (2007), Adaptive optics for enhanced signal in CARS microscopy, Optics Express, Vol. 15, No. 26, (2007), pp. 18209-18219, 1094-4087

Zeek E., Maginnis K., Backus S., Russek U., Murnane M., Mourou G., Kapteyn H., Vdovin G. (1999), Pulse compression by the use of a deformable mirror, Optics Letters, Vol. 24, No. 7, (1999), pp. (493-495), 0034-6748

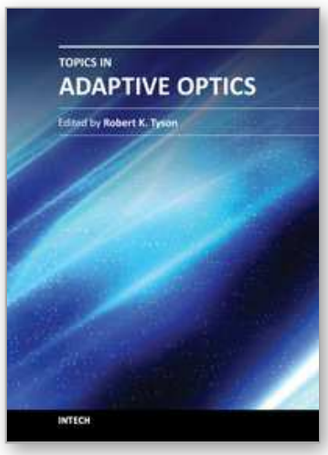

Topics in Adaptive Optics
Edited by Dr. Bob Tyson

ISBN 978-953-307-949-3
Hard cover, 254 pages
Publisher InTech
Published online 20, January, 2012
Published in print edition January, 2012

Advances in adaptive optics technology and applications move forward at a rapid pace. The basic idea of wavefront compensation in real-time has been around since the mid 1970s. The first widely used application of adaptive optics was for compensating atmospheric turbulence effects in astronomical imaging and laser beam propagation. While some topics have been researched and reported for years, even decades, new applications and advances in the supporting technologies occur almost daily. This book brings together 11 original chapters related to adaptive optics, written by an international group of invited authors. Topics include atmospheric turbulence characterization, astronomy with large telescopes, image post-processing, high power laser distortion compensation, adaptive optics and the human eye, wavefront sensors, and deformable mirrors.

InTech Europe
University Campus STeP Ri
Slavka Krautzeka 83/A
51000 Rijeka, Croatia
Phone: +385 (51) 770 447
Fax: +385 (51) 686 166
www.intechopen.com

InTech China
Unit 405, Office Block, Hotel Equatorial Shanghai
No.65, Yan An Road (West), Shanghai, 200040, China
中国上海市延安西路65号上海国际贵都大饭店办公楼405单元
Phone: +86-21-62489820
Fax: +86-21-62489821

IntechOpen